Cardiovasc Intervent Radiol (2019) 42:69–77
https://doi.org/10.1007/s00270-018-2041-x

CLINICAL INVESTIGATION INTERVENTIONAL ONCOLOGY

Utility of the Virtual Liver Parenchymal Perfusion Area Using a Commercially Available Workstation in Transarterial Chemoembolization for Hepatocellular Carcinoma

Mitsuhiro Kinoshita[1] · Katsuya Takechi[1] · Yuta Arai[2] · Ryozo Shirono[3] · Yoshihiro Nagao[4] · Shoichi Izumi[4] · Takuya Akagawa[4] · Shiori Noda[5] · Shoichiro Takao[6] · Chikara Ogawa[7] · Daisuke Suwa[8] · Katsuyoshi Tamaki[9] · Naoto Uyama[1] · Yoko Akagawa[1] · Kyosuke Osaki[1] · Norio Ohnishi[1] · Hayato Tani[1]

Received: 17 April 2018 / Accepted: 17 July 2018 / Published online: 23 July 2018

Abstract

Purpose To evaluate the accuracy of the virtual liver parenchymal perfusion area using a commercially available workstation and liver analysis software in conventional transarterial chemoembolization (cTACE) for hepatocellular carcinoma (HCC).

Materials and Methods This method was retrospectively applied to 29 treated HCCs in 23 patients. The virtual embolic area (VEA) was estimated based on cone beam computed tomography during hepatic arteriography using a commercially available workstation and liver analysis software by two observer groups (group A: experts; group B: semi-experts). The real embolic area (REA) was defined as the area where iodized oil accumulated on computed tomography at 1 week after cTACE. The REA was estimated by each of the two groups, and the mean REA between the groups (mREA) was used as a standard reference. Agreement of volume and cross-sectional area in three orthogonal planes between the VEA and mREA were analyzed using intraclass correlation coefficients (ICCs) and Bland–Altman plots.

Results The ICCs for volume between VEA and mREA were 0.97 and 0.88 for groups A and B, respectively, and those for cross-sectional area were 0.94 and 0.88 for the axial plane, 0.95 and 0.83 for the coronal plane, and 0.87 and 0.74 for the sagittal plane, respectively. Thus, the overall agreement was excellent, except for the sagittal imaging plane in group B.

✉ Mitsuhiro Kinoshita
kino3216@tokushima-med.jrc.or.jp

[1] Department of Radiology, Tokushima Red Cross Hospital, 103, Irinokuchi Komatsushima-cho, Komatsushima City, Tokushima 773-8502, Japan

[2] Department of Radiology (Diagnostic Radiology), Tokushima University Hospital, 2-50-1, Kuramoto-cho, Tokushima City, Tokushima 770-8503, Japan

[3] Department of Radiology, Kawashima-kai Kawashima Hospital, 1-39, Kitasakoichiban-cho, Tokushima City, Tokushima 770-0011, Japan

[4] Department of Radiological Technology, Tokushima Red Cross Hospital, 103, Irinokuchi Komatsushima-cho, Komatsushima City, Tokushima 773-8502, Japan

[5] Graduate School of Health Sciences, Tokushima University, 3-18-15, Kuramoto-cho, Tokushima City, Tokushima 770-8509, Japan

[6] Department of Radiology and Radiation Oncology, Institute of Biomedical Sciences, Tokushima University Graduate School, 3-18-15, Kuramoto-cho, Tokushima City, Tokushima 770-8509, Japan

[7] Department of Gastroenterology and Hepatology, Takamatsu Red Cross Hospital, 1-3, Ban-cho, Takamatsu City, Kagawa 760-0017, Japan

[8] Department of Radiological Technology, Takamatsu Red Cross Hospital, 1-3, Ban-cho, Takamatsu City, Kagawa 760-0017, Japan

[9] Department of Hepatology, Tourai-kai Okubo Hospital, 2-30, Omichi, Tokushima City, Tokushima 770-0923, Japan

Conclusion This method using a commercially available workstation and liver analysis software can be useful for estimating the embolic area in cTACE.

Keywords Cone beam computed tomography · Hepatocellular carcinoma · Transarterial chemoembolization · 3-Dimensional workstation · Real embolic area · Virtual embolic area · Virtual liver parenchymal perfusion area

Introduction

Transarterial chemoembolization (TACE) is an effective therapeutic option for unresectable hepatocellular carcinoma (HCC) [1, 2]. The success of TACE is determined by the identification of the tumor-feeding vessel and complete embolization of the entire tumor, including the safety margin [3, 4]. Development of automated tumor feeder detection (AFD) software for angiography now facilitates easy detection of tumor-feeding vessels on 3-dimensional (3-D) workstations [4–7]. However, AFD software does not show the optimal catheter position, and it is often difficult to determine the territory covered by the tumor feeder, including the normal area.

Virtual parenchymal perfusion (VPP) software shows the arterial territory [8, 9], but this is prototype software that is not yet commercially available. Therefore, we used a commercially available 3-D workstation and liver analysis software (Synapse Vincent ver. 5.2; Fujifilm, Tokyo, Japan) to estimate the liver parenchymal perfusion area [10]. This is a specific application of this workstation for operative simulations using the dominant region extraction function of the portal vein and other veins [11–14]. The purpose of this retrospective study was to evaluate the accuracy of the virtual liver parenchymal perfusion area using this workstation and software in conventional TACE (cTACE) for HCC.

Materials and Methods

Patient Selection

Between July 2016 and June 2017, 144 TACE procedures were performed in 110 patients at our hospital. The inclusion criteria for this study were (1) cTACE performed in the sub-segmental hepatic arteries or more distally (superselective or ultraselective cTACE) and not via extrahepatic collateral vessels; (2) newly developed HCC; and (3) follow-up by non-contrast-enhanced computed tomography (CT) that showed a clearly embolic area of each HCC. A total of 115 TACE procedures were excluded because of use of TACE with drug-eluting beads (n=47), non-selective cTACE (n=22), cTACE including the extrahepatic collateral vessels (n=5), superselective or ultraselective cTACE for recurrent HCC (n=36), and overlap of embolized areas of HCCs (n=5). Thus, 29 TACE procedures (29 HCCs) in 23 patients (15 men and 8 women) met the above criteria. The background of the patients is shown in Table 1. HCC was diagnosed based on nodular staining and contrast medium washout on a dynamic CT and/or dynamic magnetic resonance imaging (MRI), and nodular staining on digital subtraction angiography or cone beam CT during hepatic arteriography (CBCTHA), as well as hyperintensity on T2- and diffusion-weighted MRI. The institutional review board approved this retrospective study, and no patient consent to the study was required. All patients were informed about the benefits and potential risks of the procedure, and all provided written informed consent.

Conventional TACE

All cTACE procedures were performed via the femoral artery using an angiographic system equipped with a flat-panel detector (FPD) (Allura Xper FD 20/10; Philips Healthcare, Best, The Netherlands). First, cone beam CT during arterial portography (CBCTAP) (XperCT; Philips Healthcare) and superior mesenteric arteriography were conducted using a 5-F catheter (Twist; Medikit, Tokyo, Japan). Second, celiac arteriography was conducted using the 5-F catheter, followed by CBCTHA (XperCT; Philips Healthcare) via the common or proper hepatic artery (non-selective CBCTHA). Utilizing the celiac arteriography and CBCTHA, we find the tumor-feeding artery. An arteriogram of the tumor-feeding artery was obtained using a 1.7-F microcatheter (Asahi Veloute; Asahi Intecc, Aichi, Japan or Progreat λ; Terumo, Tokyo, Japan), which was moved into place using a 0.016-inch guidewire (Asahi Meister; Asahi Intecc). After confirming that the tumor had been stained and the tumor-feeding branch was identified, the microcatheter was inserted into the branch as selectively as possible. An epirubicin (Farmorubicin; Kyowa Hakko, Tokyo, Japan)-iodized oil (Lipiodol; Guerbet Japan, Tokyo, Japan) emulsion was slowly and carefully injected so as not to reflux until dense accumulation of iodized oil was noted in the tumor on a spot radiograph. To prepare the emulsion, 0.5–6 mL of iodized oil was mixed with 10–30 mg of epirubicin. Subsequently, gelatin sponge particles (Gelpart; Nippon Kayaku, Tokyo, Japan) were carefully injected to obstruct the tumor-feeding branch. Spot radiographs were obtained to record the catheter position in each tumor feeder and to confirm dense accumulation of iodized oil in the tumors. If the tumor was also

Table 1 Patient characteristics

Number of patients	23
Number of tumors	29
Age (year)[a]	73.8 ± 8.41 (52, 87)
Sex (male/female)	15/8
Etiology (HCV/HBV/alcohol/AIH/NASH/unkown)	12/6/2/1/1/1
Child–Pugh class (A/B)	18/5
Tumor location (S1/3/4/5/6/7/8)	2/4/2/3/6/6/6
Tumor size (mm)[a]	16.8 ± 9.1 (6.6, 40.7)

HCV hepatitis C virus, *HBV* hepatitis B virus, *AIH* autoimmune hepatitis, *NASH* non-alcoholic steatohepatitis

[a]Mean ± SD (minimum, maximum)

fed by other feeding vessels, additional cTACE procedures were performed.

Cone Beam CT

All patients underwent non-selective CBCTHA during TACE. CBCT was performed using a 38 × 30 cm FPD C-arm angiographic unit. A total of 312 projections at 120 kV and 50–325 mA were acquired over an angular range of 240° during a 5.2-s rotation of the C-arm around the patient in the expiratory phase. 3-D volume reconstructed images were shown within 3-s after acquisition. The resulting CBCT had an isotropic resolution of 0.98 mm for a 250 × 250 × 194-mm field of view (matrix size 256; pixel binning 4 × 4) and 0.49 mm for a 250 × 250 × 194-mm field of view (matrix size 512; pixel binning 4 × 4). Non-selective CBCTHA was performed on the common or proper hepatic artery with injection of 24 mL of contrast medium (Iopamiron, 370 mg of iodine per milliliter; Bayer Pharma, Osaka, Japan) at a rate of 2 mL/s through a 5-F catheter.

Estimation and Evaluation of Real Embolic Area

A Follow-up non-contrast-enhanced CT was performed 1 week after cTACE to evaluate the iodized oil distribution and complications. All images were obtained using a CT scanner (Somatom Sensation 64 Scanner; Siemens, Forchheim, Germany or Aquilion One; Canon Medical Systems, Tochigi, Japan) during the inspiratory phase. Since there is no standard method to establish real embolic area (REA), this area was defined as that in which iodized oil accumulated on CT images.

The REA was estimated by two observer groups (groups A and B) using the 3-D workstation. Each group comprised an interventional radiologist and a radiological technician, with 10 years (group A; experts: M.K. and Y.N.) or 5 years (group B; semi-experts: K.T. and S.I.) experience at performance of TACE and use of the angiography suite and 3-D workstation, respectively. The mean REA between groups A and B (mREA) was used for reference because estimation of REA is performed manually; therefore, there is a possibility that individual differences may occur. The volume and maximum cross-sectional areas of iodized oil accumulation in the tumor in the axial, coronal, and sagittal planes (Fig. 1) for the REA were measured by each group using the 3-D workstation.

Estimation and Evaluation of Virtual Embolic Area

Groups A and B used a commercial 3-D workstation and liver analysis software to estimate VEA. The CBCT images were randomized, and there was a 4-week interval between estimation and evaluation of VEA and final estimation and evaluation of REA to reduce bias. We used two groups to evaluate VEA because the procedure requires manual operation, as described below, and accuracy may differ depending on the proficiency of the user. The process of estimation and evaluation of VEA was as follows (Fig. 2). (1) Non-selective CBCTHA data were transferred to the 3-D workstation with liver analysis software. (2) Liver parenchyma were extracted manually because CBCT data cannot be used for automatic extraction, unlike CT data. The extraction method for the liver parenchyma involved enclosing the contour of the liver in several sections. If the extraction is selected, the complementary region is extracted. (3) Major hepatic arteries were extracted manually, in addition to minor ones extracted using region-growing segmentation. Eventually, volume rendering of the hepatic arteries was created. (4) A virtual injection point for each tumor feeder was selected via the 3-D arteriogram extracted from non-selective CBCTHA with reference to spot radiographs obtained during cTACE. (5) VEA images were obtained after analysis using the software in a few seconds. The total processing time required from the time the CBCT image was available to the user to completion of estimation of VEA was about 30 min. For embolization of a single tumor from multiple tumor-

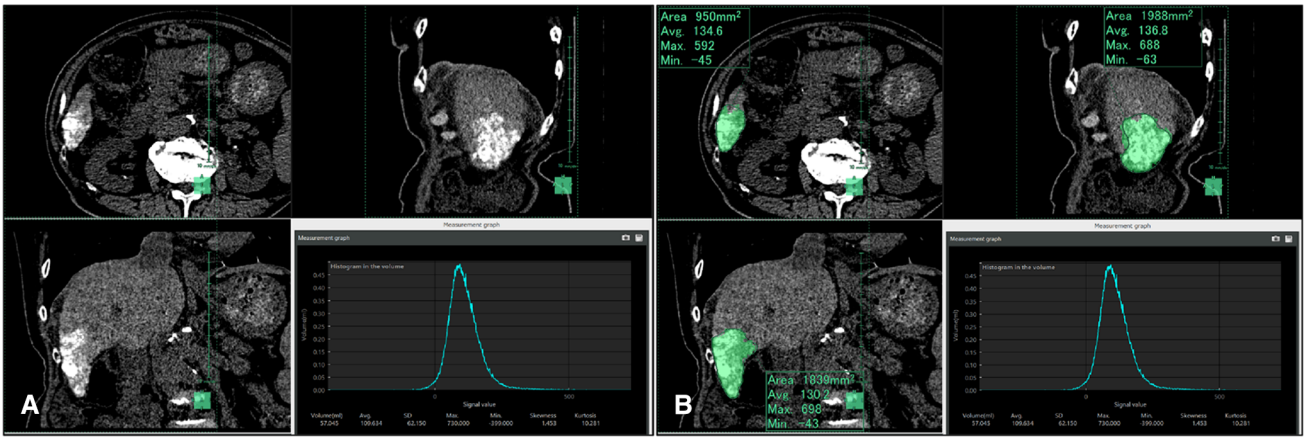

Fig. 1 Measurement of the real embolic area (REA). **A** 3-D images of the REA. **B** Measurements of the REA using a 3-D workstation: volume and cross-sectional areas in three orthogonal planes (axial, coronal, and sagittal). The curve bottom right in figure shows histogram in the volume. The vertical axis represents the volume (ml), while the horizontal axis represents the signal value (HU)

Fig. 2 Process of estimation and evaluation of the virtual embolic area (VEA) using a 3-D workstation. **A** While referencing multiplanar reconstruction non-selective CBCTHA images, liver parenchyma were extracted manually. **B** Hepatic arteries were also extracted manually. **C** HCC in S6 (open arrowhead) was also extracted, and one of the virtual injection points of tumor feeders (A6) on the 3-D arteriogram (solid arrow) was selected with reference to the spot radiographs (not shown) obtained during cTACE. **D** VEA images (solid arrowhead) were obtained after analysis by the software in a few seconds

feeding branches, the VEA was considered as the summation of VEAs for all tumor-feeding braches. Parameters for VEA similar to those for REA were measured using the 3-D workstation.

Statistical Analysis

Variables were tested for normality of distribution by using the Shapiro–Wilk test. Results are reported as mean ± standard deviation. Intraclass correlation coefficients (ICCs)

and Bland–Altman plots were used to evaluate agreement between the volume and cross-sectional areas in three orthogonal directions (axial, coronal, and sagittal) between VEA and mREA. ICC ranges from 0 to 1.00, with values closer to 1.00 representing better agreement. For each ICC, a 95% confidence interval (Cl) was calculated. The ICC value was interpreted as follows: <0.40, poor agreement; 0.40–0.59, fair agreement; 0.60–0.74, good agreement; > 0.74, excellent agreement [15]. Results of Bland–Altman plots with bias and standard deviation of the differences are reported for variability between VEA and mREA (volume, cross-sectional area in axial, coronal and sagittal planes). Analyses of ICC and Bland–Altman plots were performed using MedCalc for Windows, ver. 15.8 (MedCalc Software, Ostend, Belgium).

Results

The volume of the mREA was 101.0±61.3 mL (range 12–229 mL), and those for the VEA were 87.1±55.6 mL (13–209 mL) in group A and 88.8±57.6 mL (16–241 mL) in group B. The ICCs for volume of the mREA with those for the VEA were 0.97 (95% Cl: 0.94, 0.99) in group A and 0.88 (95% Cl: 0.77, 0.94) in group B. The axial cross-sectional area of the mREA was 2070.1±1055.7 mm^2 (472–3923 mm^2), and those for the VEA were 1971.5±1064.4 mm^2 (283–4084 mm^2) in group A and 2099.3±1134.7 mm^2 (201–5043 mm^2) in group B, with ICCs of 0.94 (95% Cl: 0.88, 0.97) and 0.88 (95% Cl: 0.77, 0.94), respectively. The respective coronal cross-sectional areas were 2134.2±1094.1 mm^2 (589–4548 mm^2), 1943.6±1050.9 mm^2 (318–4308 mm^2), and 1856.4±1001.9 mm^2 (421–4214 mm^2), with ICCs of 0.95 (95% Cl: 0.90, 0.98) and 0.83 (95% Cl: 0.68, 0.92); and the sagittal cross-sectional areas were 2205.1±1019.2 mm^2 (719–4199 mm^2), 1909.4±883.7 mm^2 (473–3776 mm^2), and 1933.3±988.7 mm^2 (443–4440 mm^2), with ICCs of 0.87 (95% Cl: 0.75, 0.94) and 0.74 (95% Cl: 0.52, 0.87), respectively.

The ICCs for volume and cross-sectional area between mREA and VEA (Tables 2 and 3) showed excellent agreement, except for the sagittal plane in group B, which was classified as good agreement. Moreover, the lower bounds of the 95% CI indicated excellent agreement, except for the coronal and sagittal planes in group B, which were in good agreement. Bland–Altman plots between VEA and mREA for volume and cross-sectional area (Figs. 4 and 5) showed no systematic biases between VEA and mREA.

Discussion

Superselective cTACE has a higher therapeutic effect than non-selective cTACE, especially for small HCCs [16–18], and also contributes to the preservation of liver reserve. Development of 3-D workstations and software for angiography has made it easier to detect tumor-feeding vessels [4–7]. However, there are no fixed standards for determining the catheter position in the tumor feeder, and this is left to the operator. Therefore, selective CBCTHA in the tumor feeder or plain CBCT after injection of the anticancer drug-iodized oil emulsion are performed to confirm the vascular territory. However, it can be difficult to perform selective CBCTHA in tumor feeders accurately because the contrast medium tends to flow out of these vessels. Selective CBCTHA requires an increase in the amount of contrast medium, and the additional CBCT leads to increased radiation exposure and procedure time. If the vascular territory of tumor-feeding arteries can be determined before chemoembolization, the optimal catheter position including the whole tumor and the safety margin for chemoembolization can be determined with reference

Table 2 ICC in volume and cross-sectional area between mREA and VEA Group A

Parameter	ICC	95% Confidence interval	
		Lower bound	Upper bound
Volume	0.97	0.94	0.99
Cross-sectional area			
Axial	0.94	0.88	0.97
Coronal	0.95	0.90	0.98
Sagittal	0.87	0.75	0.94

ICC intraclass correlation coefficients, *mREA* mean real embolic area, *VEA* virtual embolic area

Table 3 ICC in volume and cross-sectional area between mREA and VEA Group B

Parameter	ICC	95% Confidence interval	
		Lower bound	Upper bound
Volume	0.88	0.77	0.94
Cross-sectional area			
Axial	0.88	0.77	0.94
Coronal	0.83	0.68	0.92
Sagittal	0.74	0.52	0.87

ICC intraclass correlation coefficients, *mREA* mean real embolic area, *VEA* virtual embolic area

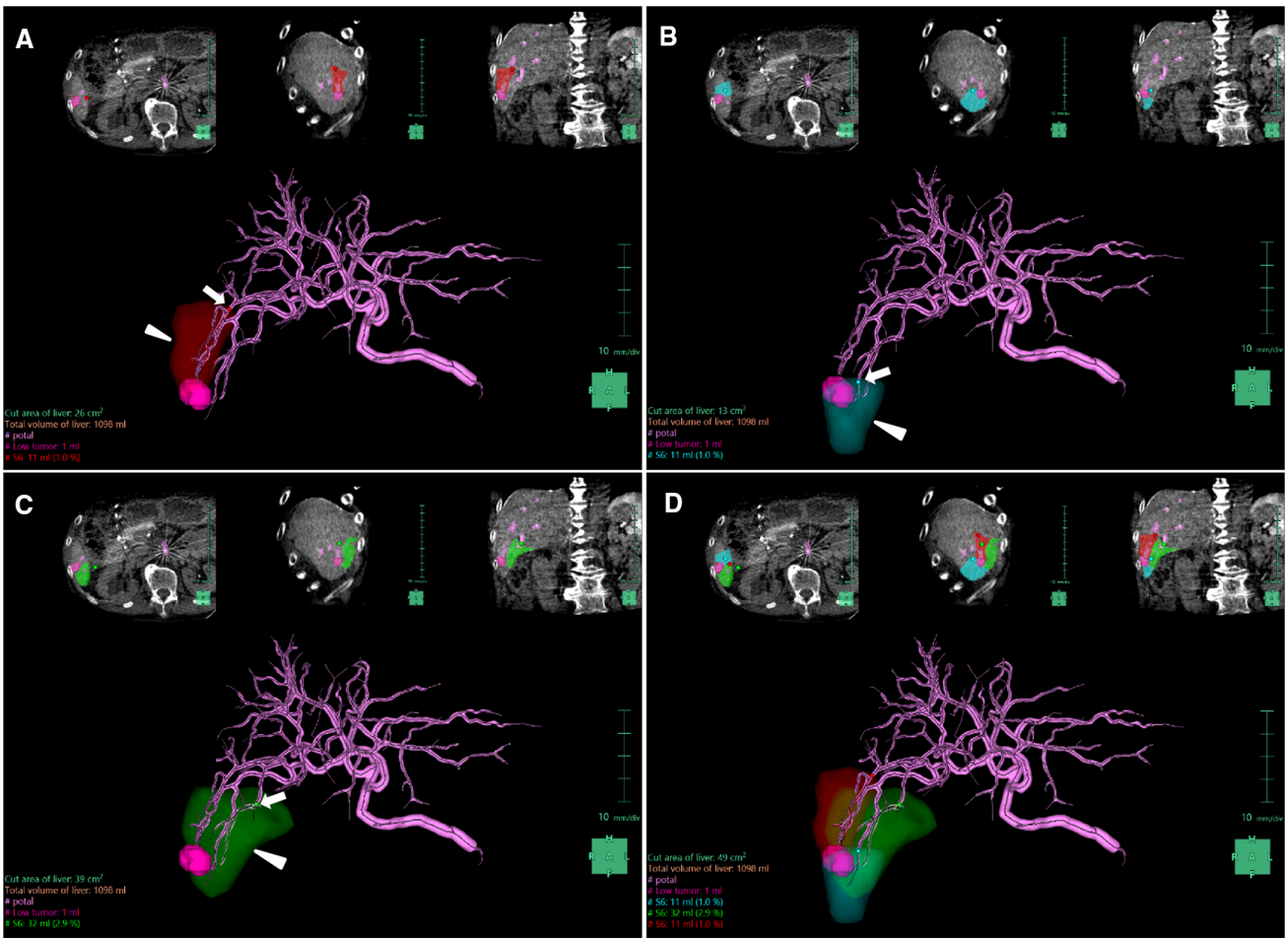

Fig. 3 An 81-year-old female with hepatocellular carcinoma (HCC) in S6. There were three feeding arteries for HCC (purple sphere) (**A**, **B**, **C**). The virtual injection points (solid arrows) of the first, second, and third feeding arteries are shown in red (**A**), blue (**B**), and green (**C**), respectively. The virtual embolic areas (VEAs) are the translucent areas (solid arrowheads) shown in red (**A**), blue (**B**), and green (**C**), respectively, on the 3-D images and on the multiplanar images in the upper part of each figure. **D** The total VEA is shown in one figure, with each volume of the VEA in the lower left of the figure

to VEA. Moreover, it may contribute to the therapeutic effects, reduce side effects, and the preservation of liver reserve, because it is possible to intensively inject more anticancer drug-iodized oil emulsion into the tumor and safety margin and to reduce its distribution and embolic area to normal liver parenchyma. In addition, reference to VEA may contribute to decreases in radiation exposure, contrast medium, and procedure time.

VPP software has excellent performance, but is still prototype software that is not commercially available. Therefore, we used commercially available liver analysis software for estimating the virtual parenchymal perfusion area on a 3-D workstation, which was originally developed for simulation of the resection range for hepatectomy [11–14]. The VEA was estimated using an algorithm based on the Voronoi tessellation [12]. This software is not written for analysis of a hepatic artery, but only for a hepatic vein or the portal vein. This software was slightly inferior to VPP software in terms of agreement [8]. However, it was superior to VPP software in that the VEA had clear divisions with the non-embolic area. In addition, when there are multiple tumor feeders, it is possible to display all of the donor areas separately and with color coding (Fig. 3). These are impossible with VPP software.

The agreement between VEA and mREA was excellent for both groups in the study. However, the agreement for group B (semi-experts) was somewhat inferior to that for group A (experts). One reason for this is that VEA was estimated manually and it was difficult to identify and extract a fine hepatic artery in the process. This most likely was influenced by the difference in experience of the planner. However, even for group B, a satisfactory result was obtained and this indicates that a certain accuracy is possible for a user with some experience of estimating VEA. The volumes of VEA and mREA were in excellent agreement in most tumors. However, the volume of mREA

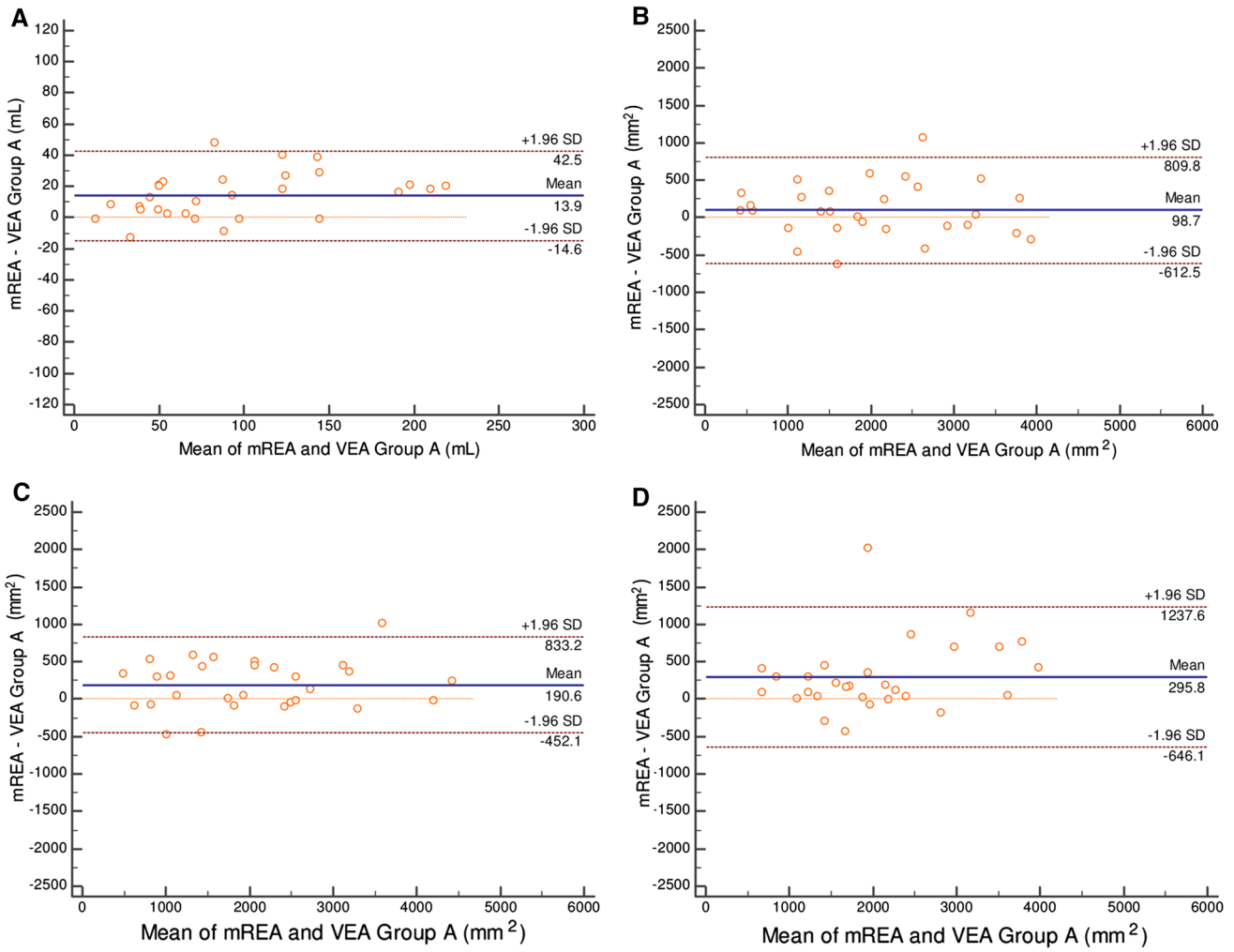

Fig. 4 Bland–Altman plots showing agreement between the mean real embolic area (mREA) and the virtual embolic area (VEA) in group A. The blue line is the mean difference in volume or cross-sectional area between the mREA and VEA. Dotted brown lines indicate ± 1.96 standard deviations (SD). The dotted red line is zero. **A** Volume. **B** Axial cross-sectional area. **C** Coronal cross-sectional area. **D** Sagittal cross-sectional area

was larger than that found for VEA in 23 tumors (79.0%) in group A and in 20 tumors (69.0%) in group B (Figs. 4 and 5). This may be explained through artery to artery communications and an artery to portal vein network through arterioportal communications, and tumor drainage. In addition, there is a possibility that there is some reflux of the anticancer drug-iodized oil emulsion during injection. The cross-sectional areas of VEA and mREA were also in excellent agreement with most tumors. However, the ICCs for cross-sectional areas were slightly lower than those for volume, especially in the sagittal plane. In this study, CBCTHA was performed in the expiratory phase, whereas follow-up CT was performed in the inspiratory phase. Therefore, the liver shape differed between CBCTHA and follow-up CT, and this may have had a greater influence on the cross-sectional areas than on volume, especially for the area in the sagittal plane.

A great improvement in estimating the virtual parenchymal perfusion area is required for practical clinical use. Shortening of the time required to prepare a simulation is needed. Customization of the workstation made it possible to estimate VEA in about 30 min. Automatic extraction of liver parenchyma and hepatic arteries from CBCT data might shorten this time to less than half, in addition to improving accuracy and standardizing results.

This study has several limitations. First, tumor control and degree of preservation of liver reserve are not obtained by referencing VEA. In addition, the study was retrospective and included only newly developed tumors. A prospective and long-term follow-up study that includes recurrent tumors is necessary to evaluate clinical use. Second, CBCT data were used to estimate VEA, but it may have been more effective to use CT data. However, when CT data are used, an interventional radiology (IVR)-CT

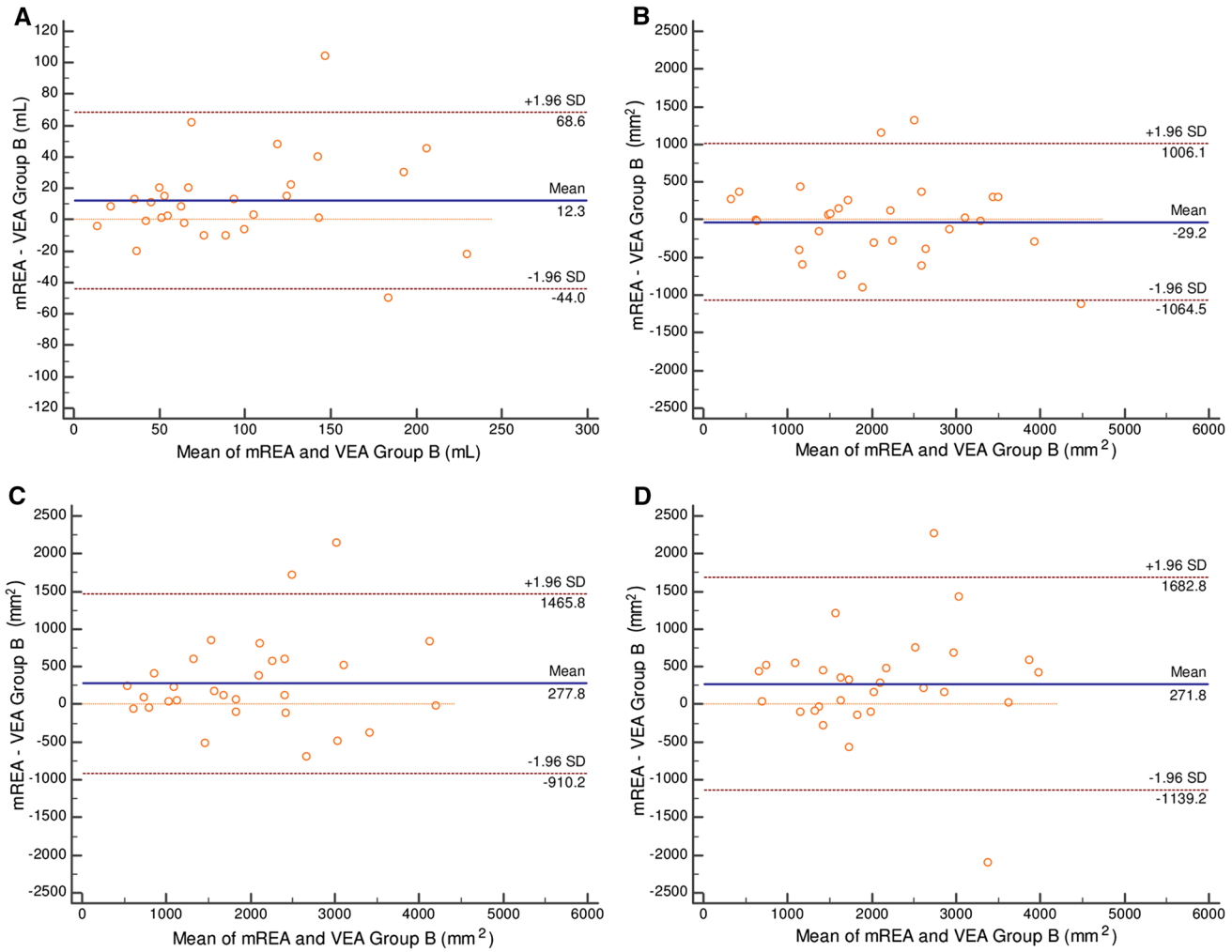

Fig. 5 Bland–Altman plots showing agreement between the mean real embolic area (mREA) and the virtual embolic area (VEA) in group B. The blue line is the mean difference in volume or cross-sectional area between the mREA and VEA. Dotted brown lines indicate ± 1.96 standard deviations (SD). The dotted red line is zero. **A** Volume. **B** Axial cross-sectional area. **C** Coronal cross-sectional area. **D** Sagittal cross-sectional area

system or conventional CT is needed. There are IVR-CT systems installed in only a limited number of institutions. Otherwise, conventional CT is common, but its use requires a move from the angiographic site to the CT room. Third, REA was defined as the area in which iodized oil accumulated on a follow-up CT performed 1 week after cTACE. It is more accurate to perform CBCT or CT immediately after cTACE because a follow-up CT performed 1 week after cTACE has to take into account iodized oil washout and to use selective CBCTHA, rather than a follow-up CT performed 1 week after cTACE. However, the distribution of small amounts of iodized oil in CBCT may be ambiguous. Although a follow-up CT performed immediately after cTACE can evaluate iodized oil accumulation, it is difficult to evaluate side effects such as the appearance of ascites. Therefore, a follow-up CT performed 1 week after cTACE seemed to be reasonable. Fourth, the agreement between VEA and REA depends on the planner because estimating VEA is performed manually. However, all estimations of VEA were performed by two groups, and agreements in parameters for VEA and REA were excellent for the most part.

In conclusion, VEA based on CBCT data using a commercially available 3-D workstation and liver analysis software in cTACE can be displayed using color coding and clear divisions, and VEA showed good agreement with REA retrospectively. This method can be useful for estimating the embolic area in cTACE. However, at present, it takes time to process data. Therefore, further improvements are needed and several problems remain to be solved before use of this new method can be recommended in clinical practice.

Acknowledgements The authors would like to thank Yoshihiro Okayama (Clinical Trial Center for Development Therapeutics, Tokushima University Hospital) for his assistance with statistical analysis.

Compliance with Ethical Standards

Conflict of interest The authors declared that they have no conflict of interest.

Ethical Approval All procedures performed in studies involving human participants were in accordance with the ethics of the institutional and/or national research committee and with the 1964 Helsinki declaration and its later amendments or comparable ethical standards.

Informed Consent Informed consent was obtained from all individual participants included in the study.

References

1. Llovet JM, Bruix J. Systematic review of randomized trials for unresectable hepatocellular carcinoma: chemoembolization improves survival. Hepatology. 2003;37:429–42.
2. Lo CM, Ngan H, Tso WK, Liu CL, Lam CM, Poon RT, Fan ST, Wong J. Randomized controlled trial of transcatheter lipiodol chemoembolization for unresectable hepatocellular carcinoma. Hepatology. 2002;35:1164–71.
3. Miyayama S, Yamashiro M, Hashimoto M, Hashimoto N, Ikuno M, Okumura K, Yoshida M, Matsui O. Comparison of local control in transcatheter arterial chemoembolization of hepatocellular carcinoma≤6 cm with or without intraprocedural monitoring of the embolized area using cone-beam computed tomography. Cardiovasc Intervent Radiol. 2014;37:388–95.
4. Miyayama S, Yamashiro M, Hashimoto M, Hashimoto N, Ikuno M, Okumura K, Yoshida M, Matsui O. Identification of small hepatocellular carcinoma and tumor-feeding branches with cone-beam CT guidance technology during transcatheter arterial chemoembolization. J Vasc Interv Radiol. 2013;24:501–8.
5. Miyayama S, Yamashiro M, Ikuno M, Okumura K, Yoshida M. Ultraselective transcatheter arterial chemoembolization for small hepatocellular carcinoma guided by automated tumor-feeders detection software: technical success and short-term tumor response. Abdom Imaging. 2014;39:645–56.
6. Iwazawa J, Ohue S, Hashimoto N, Muramoto O, Mitani T. Clinical utility and limitations of tumor-feeder detection software for liver cancer embolization. Eur J Radiol. 2013;82:1665–71.
7. Ronot M, Abdel-Rehim M, Hakimé A, Kuoch V, Roux M, Chiaradia M, Vilgrain V, de Baere T, Deschamps F. Cone-beam CT angiography for determination of tumor-feeding vessels during chemoembolization of liver tumors: comparison of conventional and dedicated-software analysis. J Vasc Interv Radiol. 2016;27:32–8.
8. Miyayama S, Yamashiro M, Nagai K, Yokka A, Yoshida M, Sakuragawa N. Performance of novel virtual parenchymal perfusion software visualizing embolized areas of transcatheter arterial chemoembolization for hepatocellular carcinoma. Hepatol Res. 2017;47:446–54.
9. Derbel H, Kobeiter H, Pizaine G, Ridouani F, Luciani A, Radaelli A, Van der Sterren W, Chiaradia M, Tacher V. Accuracy of a cone-beam CT virtual parenchymal perfusion algorithm for liver cancer targeting during intra-arterial therapy. J Vasc Interv Radiol. 2018;29:254–61.
10. Ogawa C, Minami Y, Morita M, Noda T, Arasawa S, Izuta M, Kubo A, Matsunaka T, Tamaki H, Shibatoge M, Kudo M. Prediction of embolization area after conventional transcatheter arterial chemoembolization for hepatocellular carcinoma using SYNAPSE VINCENT. Dig Dis. 2016;34:696–701.
11. Saito S, Yamanaka J, Miura K, Nakao N, Nagao T, Sugimoto T, Hirano T, Kuroda N, Iimuro Y, Fujimoto J. A novel 3D hepatectomy simulation based on liver circulation: application to liver resection and transplantation. Hepatology. 2005;41:1297–304.
12. Takamoto T, Hashimoto T, Ogata S, Inoue K, Maruyama Y, Miyazaki A, Makuuchi M. Planning of anatomical liver segmentectomy and subsegmentectomy with 3-demensional simulation software. Am J Surg. 2013;206:530–8.
13. Ohshima S. Volume analyzer SYNAPSE VINCENT for liver analysis. J Hepatobiliary Pancreat Sci. 2014;21:235–8.
14. Oshiro Y, Yano H, Mitani J, Kim S, Kim J, Fukunaga K, Ohkohchi N. Novel 3-dimensional virtual hepatectomy simulation combined with real-time deformation. World J Gastroenterol. 2015;21:9982–92.
15. Oppo K, Leen E, Angerson WJ, Cooke TG, McArdle CS. Doppler perfusion index: an interobserver and intraobserver reproducibility study. Radiology. 1998;208:453–7.
16. Miyayama S, Matsui O, Yamashiro M, Ryu Y, Kitao K, Ozaki K, Takeda T, Yoneda N, Notsumata K, Toya D, Tanaka N, Mitsui T. Ultraselective transcatheter arterial chemoembolization with a 2-F tip microcatheter for small hepatocellular carcinoma: relationship between local tumor recurrence and visualization of the portal vein with iodized oil. J Vasc Interv Radiol. 2007;18:365–76.
17. Miyayama S, Mitsui T, Zen Y, Sudo Y, Yamashiro M, Okuda M, Yoshie Y, Sanada T, Notsumata K, Tanaka N, Matsui O. Histopathological findings after ultraselective transcatheter arterial chemoembolization for hepatocellular carcinoma. Hepatol Res. 2009;39:374–81.
18. Iwamoto S, Yamaguchi T, Hongo O, Iwamoto H, Sanefuji H. Excellent outcomes with angiographic subsegmentectomy in the treatment of typical hepatocellular carcinoma: a retrospective study of local recurrence and long-term survival rates in 120 patients with hepatocellular carcinoma. Cancer. 2010;116:393–9.